pH-Sensitive Photoinduced Energy Transfer from Bacteriorhodopsin to Single-Walled Carbon Nanotubes in SWNT–bR Hybrids

Karim El Hadj, Patricia Bertoncini,* and Olivier Chauvet

Institut des Matériaux Jean Rouxel, Nantes Université, CNRS 2 Rue de la Houssinière, BP 32229, 44322 Nantes, France

ABSTRACT Energy transfer mechanisms in noncovalently bound bacteriorhodopsin/single-walled carbon nanotube (SWNT) hybrids are investigated using optical absorption and photoluminescence excitation measurements. The morphology of the hybrids was investigated by atomic force microscopy. In this study, proteins are immobilized onto the sidewall of the carbon nanotubes using a sodium cholate suspension–dialysis method that maintains the intrinsic optical and fluorescence properties of both molecules. The hybrids are stable in aqueous solutions for pH ranging from 4.2 to 9 and exhibit photoluminescence properties that are pH-dependent. The study reveals that energy transfer from bacteriorhodopsin to carbon nanotubes takes place. So, at pH higher than 5 and up to 9, the SWNTs absorb the photons emitted by the aromatic residues of the protein, inducing a strong increase in intensity of the E_{11} emissions of SWNTs through their E_{33} and E_{44} excitations. From pH = 4.2 to pH = 5, the protein fluorescence is strongly quenched whatever the emission wavelengths, while additional fluorescence features appear at excitation wavelengths ranging from 660 to 680 nm and at 330 nm. The presence of these features is attributed to a resonance energy transfer mechanism that has an efficiency of 0.94 ± 0.02. More, by increasing the pH of the dispersion, the fluorescence characteristics become those observed at higher pH values and *vice versa*.

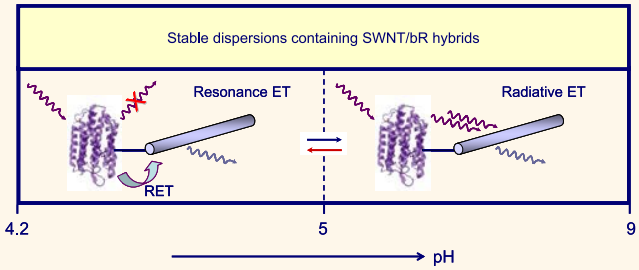

KEYWORDS: single-walled carbon nanotubes · bacteriorhodopsin · biohybrids · fluorescence · energy transfer

Understanding and controlling light-absorbing or -emitting molecule–single-walled carbon nanotube (SWNTs) interactions for sensing,[1] optoelectronics,[2] or *in vitro* and *in vivo* applications[3−6] are rapidly developing research fields. In the particular case of biomedical imaging, studies are often conducted using multiple fluorescent protein labeling. The question of the optical interaction or energy transfer between the emitting protein or fluorescent molecule and the SWNTs is therefore of prime importance. The purpose of this paper is to address this question.

Most of the works use organic dyes,[7−10] semiconducting nanoparticles/quantum dots,[11] and conjugated polymers[12,13] that are coupled to SWNTs, and they study the energy transfer involved in these systems. Only a few studies deal with photosynthetic proteins. Among them, M. Dorogi *et al.*[14] demonstrated that a photosynthetic reaction center pigment protein complex (a redox-active enzyme in which light energy initiates a chain of intra-protein electron transport reactions) is able to attach to SWNTs and that light-induced absorption changes occur. S. Kaniber *et al.*[15] showed that photosystem I proteins form active electronic junctions with carbon nanotubes. The group of M. S. Strano[16] reported the reversible assembly/disassembly capabilities of an oriented complex constituted by photosynthetic reactions centers, recombinant proteins, phospholipids, and SWNTs. The components self-assemble into a configuration in which an array of lipid bilayers aggregates on the surface of the carbon nanotube, creating a platform for the attachment of light-converting proteins. Only in the assembled state do the complexes exhibit photoelectrochemical activity. Though photosynthetic proteins are a source

* Address correspondence to Patricia.Bertoncini@cnrs-imn.fr.

Received for review June 19, 2013 and accepted September 8, 2013.

Published online September 09, 2013
10.1021/nn403092r

of biological material well suited to technological applications, they exhibit light-induced charge transfer across lipid membranes that can be exploited for the construction of photo-optical electrical devices, are naturally abundant and readily available, and possess structure, function, and mode of energy conversion that differ across the photosynthetic evolutionary scale, allowing their use for different applications in photonics.[17]

Here bacteriorhodopsin (bR) has been chosen as the photosensitive protein. bR is the key protein for halobacterial photosynthetic capabilities, enabling the organisms to use light energy directly to drive bioenergetic processes by the generation of a proton gradient.[18] It consists of 248 residues that are arranged in seven α-helical bundles inside the lipid membrane and form a cage where a retinylidene molecule is located. This molecule and the inner shell of interacting amino acids form the chromophoric group of bR. In a preliminary study,[19] we provided evidence that the membrane bR proteins can be immobilized onto SWNTs through hydrophobic interactions between the bR α-helices and the sidewall of the nanotubes. Nevertheless, the sample preparation method we used led to very low-concentrated dispersions. For this reason, in this work, we choose to follow the sodium cholate suspension–dialysis method described by N. R. Palwai *et al.*[20] So bR proteins are noncovalently immobilized onto the sidewall of SWNTs in a way that preserves the intrinsic properties of both molecules. This study focuses on the fluorescence properties of SWNT–bR hybrids as a function of the pH. It reveals energy transfer from bR to SWNTs in the hybrids.

RESULTS AND DISCUSSION

Figure 1 displays the Raman/emission spectra of raw SWNTs (spectrum 1) and supernatants at pH 4.5 (spectrum 2) and at pH 7.5 (spectrum 3). These spectra have been obtained with an excitation line at 1064 nm. This excitation line corresponds to allowed optical E_{11} transitions of semiconducting SWNTs. The Raman resonant peaks are labeled with stars in Figure 1. The two main peaks are due to the radial breathing mode (at 268 cm^{-1}) and to the tangential G modes close to 1590 cm^{-1}. The peak close to 2551 cm^{-1} is the second-order D′ mode. There is no significant modification of the Raman line positions within our experimental accuracy. It can be noticed that two broad lines found around 550 and 1500 cm^{-1} (below the Raman G lines) are appearing (indicated by arrows in Figure 1). These lines correspond to fluorescence lines associated with the near-infrared (NIR) emission of semiconducting SWNTs, according to the pioneering work of M. J. O'Connell *et al.*[21] The NIR emission is observed for isolated semiconducting SWNTs only. In fact, when the nanotubes are embedded in bundles, the emission is quenched as soon as the bundle contains metallic

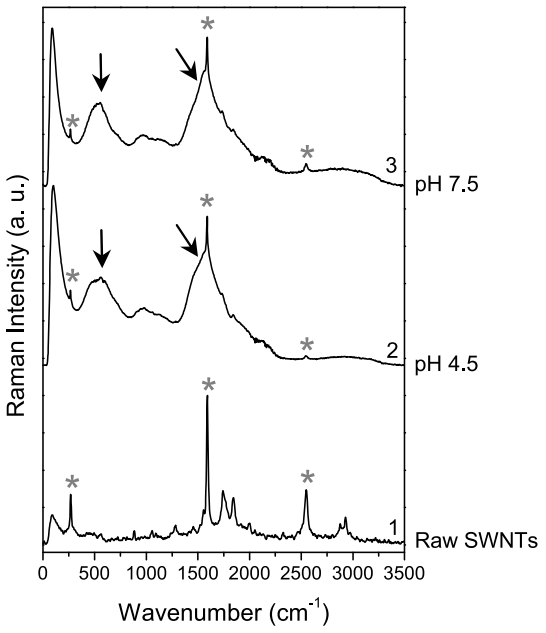

Figure 1. Raman/emission spectra of SWNT–bR hybrids at pH 7.5 (3) and at pH 4.5 (2) and raw SWNTs dispersed in ethanol (1). The spectra have been obtained with an excitation line at 1064 nm. The stars refer to the Raman resonant peaks of the SWNTs. The arrows indicate NIR fluorescence lines. The spectra have been normalized to the G band and shifted vertically for clarity.

nanotubes. The fluorescence comes from the radiative decay of the excitons formed after the absorption of the E_{11} photon. Each SWNT species should thus give a specific fluorescence line. Here, the lines at 554 and 1556 cm^{-1} may be attributed to (9,2) and (11,1) SWNTs according to S. M. Bachilo *et al.*[22] It is noteworthy that as-produced nanotubes are embedded in nonfluorescent bundles. In aqueous media, even if sonication is able to destroy the bundle organization, the hydrophobic character of the carbon surface results usually in the bundle re-formation. Note also that, in the same dialysis conditions as those used for the preparation of the dispersions containing bR, a suspension of SWNTs dispersed using sodium cholate molecules is completely destabilized (no individualized SWNT is detected any more). It turns out that the presence of the proteins is mandatory for maintaining the SWNTs dispersed in the aqueous buffer solutions.

Figure 2A and B show typical AFM images of rinsed film supernatants obtained using the intermittent contact mode in aqueous buffer. SWNTs and bR proteins can be seen on top of flat mica surfaces. Corresponding height profiles recorded along the carbon nanotubes are shown in Figure 2C and D, respectively. They exhibit irregularities due to the presence of the proteins. The heights are between 1.5 and 6 nm. These observations are consistent with the formation of SWNT–bR hybrids. The lengths of the carbon nanotubes are relatively short, 550 and 385 nm in the case of Figure 2C and D, respectively. This is likely due to the

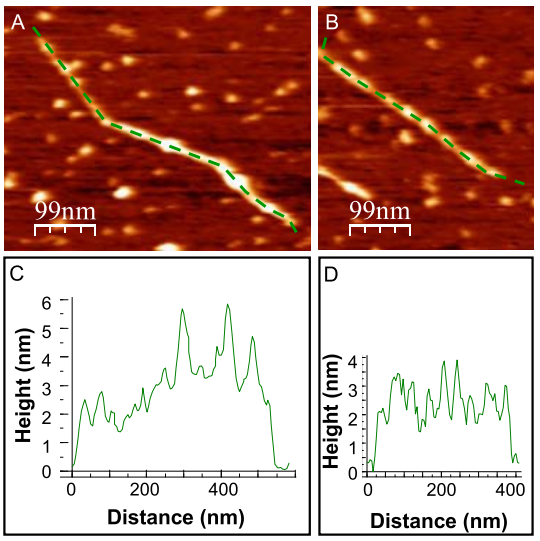

Figure 2. (A and B) AFM topographs showing individual SWNT−bR hybrids and bR proteins deposited onto a mica surface. Measurements were taken in intermittent contact mode in buffer solution at pH 4.5. Full-color *Z*-scale: 4 nm. (C and D). Section analysis profiles along the dashed green line on images (A) and (B), respectively.

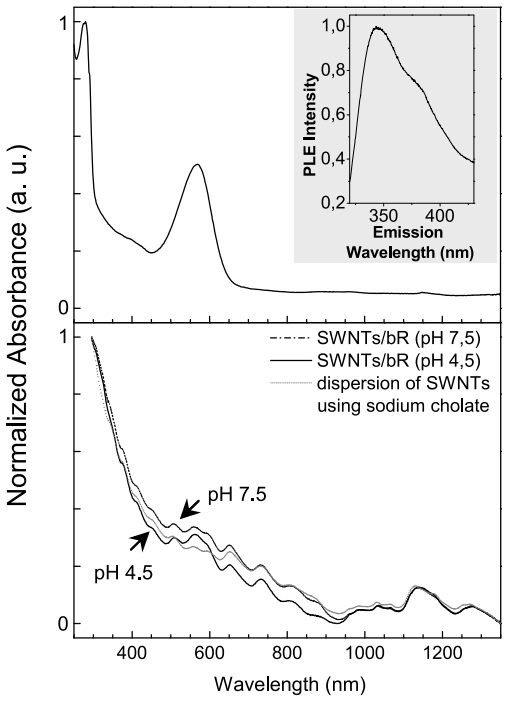

Figure 3. Upper panel: UV−visible spectra of native bR between 250 and 1350 nm. The optical absorbance is normalized at a wavelength of 280 nm. Inset: Fluorescence spectrum corresponding to the emission of the tryptophan residues of bR with an excitation wavelength of 288 nm. Bottom panel: Normalized UV−visible absorption spectra of supernatants containing individualized SWNTs dispersed by anionic surfactant molecules of sodium cholate at pH 7.5 (dotted gray line) and containing SWNTs−bR hybrids at pH 7.5 (dashed black line) and at pH 4.5 (solid black line) between 250 and 1350 nm. The optical absorbance is normalized at a wavelength of 295 nm for all spectra.

sonication step used to disperse the carbon nanotubes. By measuring their lengths on several AFM topographical images, a length of 432 ± 36 nm (average value ± standard deviation, $N = 81$) has been found.

A UV−visible absorption spectrum of native membranes containing bR is shown in the upper part of Figure 3. Absorption bands of bR are visible with two maxima occurring at ∼280 and 568 nm. The first maximum is due to the presence of aromatic residues in the protein (tryptophan and tyrosine), and the second one is related to the chromophoric group of bR.[23] A typical fluorescence emission spectrum of bR can be seen in the inset of Figure 3. The spectral characteristics are typical for tryptophan residues.[23] UV−visible absorption spectra of supernatants containing SWNT−bR hybrids at pH 7.5 (dashed black line) and pH 4.5 (solid black line) are presented in the bottom part of Figure 3. A spectrum of the initial SWNT dispersion (SWNTs individualized using sodium cholate molecules) can also be seen (dotted gray line). Separated absorption features characteristic of well-dispersed SWNTs[21] are present in all supernatants. For those containing the SWNT−bR hybrids, an increase of the absorption signal is visible at wavelengths around 568 nm, which is due to protein absorption. The protein absorbance can be evaluated by subtracting the contributions of SWNTs to the absorption signal. Thus, the optical absorption measurements allow us to evaluate the concentrations of SWNTs and bacteriorhodopsin in each sample (for details, see Methods). In addition the presence of the absorption peak at around 568 nm (the exact position depends on pH[24,25]) indicates that the retinal is still inside the core of the protein (the unbound retinal absorbs at 370 nm).[23] Another way to check the integrity of the protein in the supernatants is to measure the fluorescence emitted by the aromatic residues of the protein, essentially the tryptophan residues, in the presence and in absence of light. Fluorescence spectra were recorded in the region of emission of tryptophan residues (320 to 425 nm) with an excitation wavelength of 288 nm in the dark and under illumination in the region of the absorption of the chromophoric group of the protein. A systematic decrease of the intensity of the fluorescence emission is observed when the sample is illuminated. This behavior is well known for bacteriorhodopsin and is related to the formation of a 412 nm absorbing complex which is not present in the dark.[23] As a resume, the UV−visible spectroscopy measurements indicate that the SWNTs maintain their intrinsic optical properties when proteins are coupled to them.

The NIR emissions from various SWNT species were recorded with excitation wavelengths ranging from 300 to 750 nm. Figure 4 shows the photoluminescence excitation/emission (PLE) maps for SWNT−bR hybrids in aqueous dispersions at pH 7.5 (A) and pH 4.5 (B). (For comparison, a typical PLE map for a dispersion of

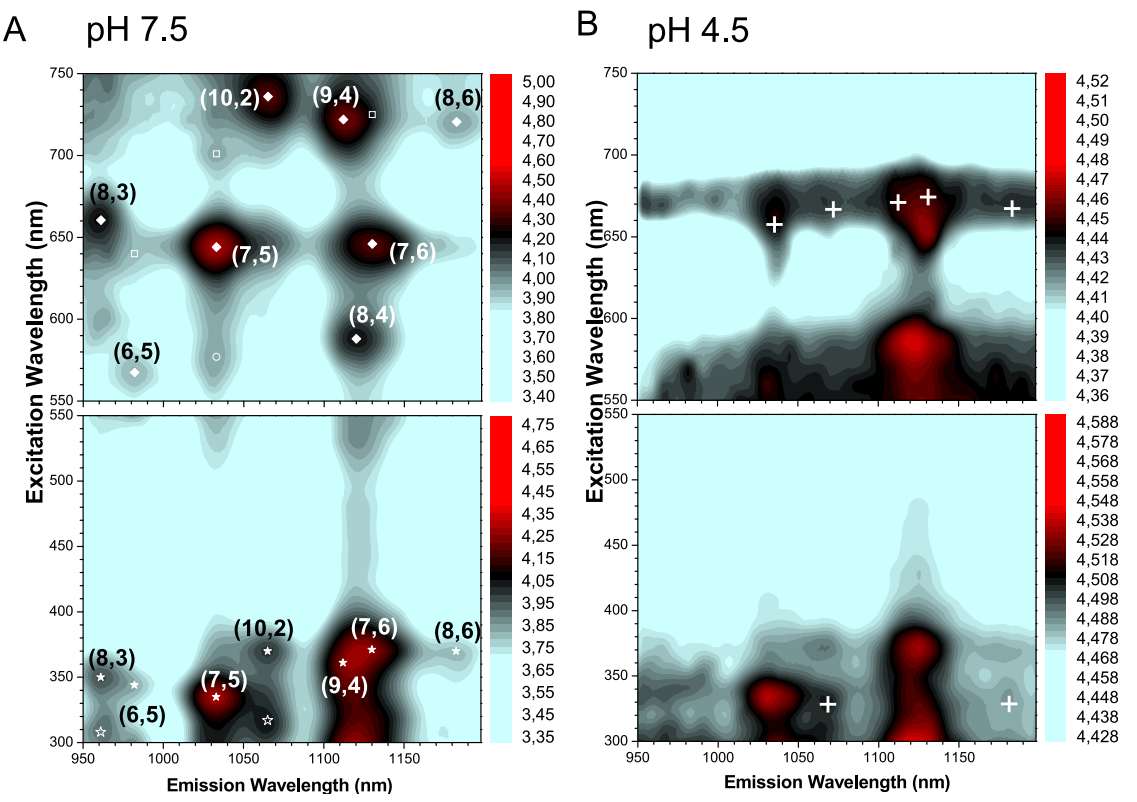

Figure 4. PLE maps of a dispersion containing SWNT/bR hybrids at pH 7.5 (A) and pH 4.5 (B). Eight species are noted: (6,5), (8,4), (8,3), (7,5), (7,6), (10,2), (9,4), and (8,6). Solid diamonds and solid and open stars represent the E_{11} emissions of SWNTs through their E_{22}, E_{33}, and E_{44} excitations, respectively. The open circle indicates a phonon sideband. Open squares denote $E_{12,21}$ transverse photoexcitations. White crosses show where nonradiative energy transfer occurs. PL intensities are logarithmically scaled. Data are presented at equal concentrations of SWNTs and bR.

SWNTs using sodium cholate molecules can be seen in Figure S3 of the Supporting Information.) On the basis of the emission wavelength from the first van Hove band gap (E_{11}) and the excitation wavelength from their second, third, and fourth van Hove band gaps (E_{22}, E_{33}, and E_{44}),[26,27] eight major SWNT chiral species, (6,5), (8,4), (8,3), (7,5), (7,6), (10,2), (9,4), and (8,6), are identified in Figure 4 as solid diamonds and solid and open stars. One G-phonon-coupled PLE satellite is indicated by an open circle.[28] Photoluminescence features located above $E_{22} \rightarrow E_{11}$ optical transition peaks have been attributed to cross-interband $E_{12,21}$ photoexcitations.[29,30] Their intensities are about 10 times weaker than the primary $E_{22} \rightarrow E_{11}$ optical transitions.[31] The PLE map for SWNT–bR hybrids in aqueous dispersions at pH 9 is similar to the one at pH 7.5 (not shown). The PLE measurements exhibit characteristic features of individualized SWNTs in a pH range from pH 4.2 to 9.

If PLE maps for SWNT–bR hybrids are quite similar at pH 7.5 and 9, new fluorescence spots appear at pH lower than 5. These additional features can be seen on the PLE map shown in Figure 4B and are indicated by crosses. Emission occurs from nanotube species present when excitation wavelengths are in the range 660–680 nm and at 330 nm, as can be seen in Figure 4B. These spectral areas do not correspond to any known active electronic transitions of the SWNTs. The position and excitation profile of the emission do, however, closely match the optical absorbance maxima of the protein at pH 4.5, as shown in the PLE maps for bR alone, as can be seen in Figure 5.

Interestingly, fluorescence intensity of bacteriorhodopsin in the visible–NIR region starts to increase when the pH becomes smaller than approximately 5.5.[25] (The PLE intensity of bR suspensions as a function of the pH is shown in Figure S2 of the Supporting Information.) PLE intensity maxima of bR alone at a given concentration are shown as a function of excitation and emission wavelengths for pH 7.5 and 4.5 in Figure 6 as black dots. Differences in intensity are clearly visible as a function of the pH and are dependent on the excitation wavelengths. In particular, at pH 4.5 the fluorescence intensity is strongly enhanced compared to pH values higher than 5. A greater spectral overlap exists between the emission of the bR and the absorption of several SWNT chiral species. To visualize this, we indicate the absorption wavelengths of several SWNT chiral species using short gray lines on the PLE maps of bR in Figure 5. All these observations are in favor of an energy transfer from photoexcited bR to the SWNTs at the lowest pH values. One way to ensure the role of bacteriorhodopsin is to bleach it and see what happens. For this, we add hydroxylamine to the dispersions containing the SWNT–bR hybrids upon illumination in order

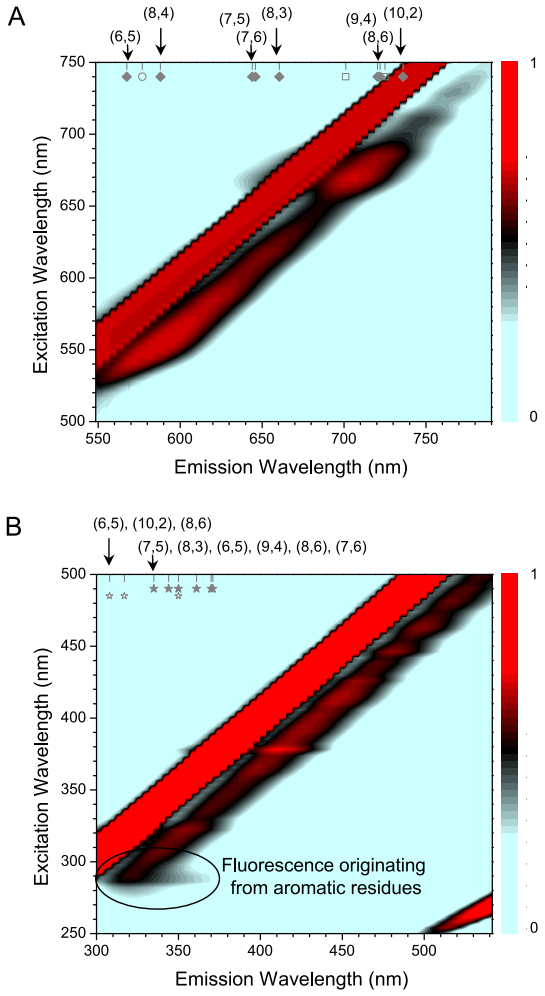

Figure 5. PLE maps of a suspension of bR at pH 4.5 with excitation wavelengths ranging from 500 to 750 nm (A) and from 250 to 500 nm (B). Absorption wavelengths of several SWNT chiral species are indicated by short gray lines. Solid diamonds and solid and open stars are related to E_{11} emissions of SWNTs through their E_{22}, E_{33}, and E_{44} excitations, respectively. Open squares denote $E_{12,21}$ transverse photoexcitations. The bright red lines where the emission wavelength is almost equal to or twice the excitation wavelength are primarily experimental artifacts caused by the lack of rejection of the excitation source. The conditions of data recording are different between the two PLE maps.

to produce a chromophore-free protein.[32,33] Thus we record PLE maps in the region of the emission of the SWNTs after the injection of hydroxylamine into the dispersions containing the SWNT–bR hybrids. These PLE maps are characteristic of a dispersion of SWNTs using sodium cholate as surfactant without the additional features previously observed. Within the first two hours, no luminescence is detected anymore. After two hours, the dispersions are completely destabilized and black aggregates are observable by eye. Therefore, additional features on the PLE map at pH 4.5 can be attributed to the presence of bacteriorhodopsin and are due to the intrinsic properties of the protein.

The intensity of the PLE peaks of the SWNT species is modified in the presence of bacteriorhodopsin and is pH-dependent. The fluorescence intensity was measured at different positions of the PLE map and normalized to the difference between fluorescence intensity maximum and minimum of the PLE map. This value is called I_r. The ratio R between I_r values for a solution containing SWNT–bR hybrids at each pH and for SWNTs dispersed using sodium cholate molecules at pH 7.5 was calculated. R values are presented in Figure 7 as bar graphs. The upper and bottom parts of Figure 7 show the data for PLE features with excitation wavelengths ranging from 550 to 750 nm and from 300 to 550 nm, respectively. Concerning the E_{11} emissions of SWNTs through their E_{22} excitations (indicated by solid diamonds) and the $E_{12,21}$ transverse photoexcitations (indicated by open squares), only small changes in intensity are recorded for dispersions containing SWNT–bR hybrids compared to a dispersion of SWNTs using sodium cholate molecules. On the contrary, the intensities of the E_{11} emissions through the E_{33} and E_{44} excitations (indicated by solid and open stars, respectively) are strongly enhanced whatever the pH of the solutions with an increase in intensity at pH 4.5, which is approximately twice the one at pH 7.5. In the case of the additional PLE spots observed at pH 4.5, seven positions indicated by white crosses in Figure 4B can be attributed to energy transfer from bR to SWNT species (7,5), (10,2), (9,4), (7,6), and (8,6). For these features, the intensity is multiplied by 2 at pH 4.5 compared to that at pH 7.5. For excitation wavelengths between 300 and 400 nm, the intensity of the near-infrared emissions of fluorescence spots is increased by a factor ranging from 3 to 9 compared to a dispersion of SWNTs using sodium cholate as surfactant. The study of the donor emission (*i.e.*, the emission of the protein) reveals that a quenching of the PLE signal of bR occurs in the presence of SWNTs.

To go deeper into the energy transfer mechanisms, the PLE maxima of the protein were measured as a function of the excitation and emission wavelengths for bR in the presence of SWNTs in the SWNT–bR hybrids at both pH and for equal concentrations in protein. The results are presented in the graphs of Figure 6. At pH 7.5, the donor emission is modified in the region of spectral overlap. (Two PLE maps in the UV–visible spectral region can be seen in Figure S3 in the Supporting Information, one for bR alone (A) and the other for SWNT–bR hybrids (B), both taken at pH 7.5.) The decrease of the steady-state fluorescence intensity is localized in the region where a spectral overlap occurs between the emission of the tryptophan residues of the protein and the absorption of the E_{33} and E_{44} excited states of the SWNTs. These observations are in favor of a radiative energy transfer. At pH 4.5, the shape of the fluorescence spectra for bR alone and in the presence of SWNTs is unchanged, while the steady-state fluorescence intensity strongly decreased whatever the emission wavelengths, as can be seen in

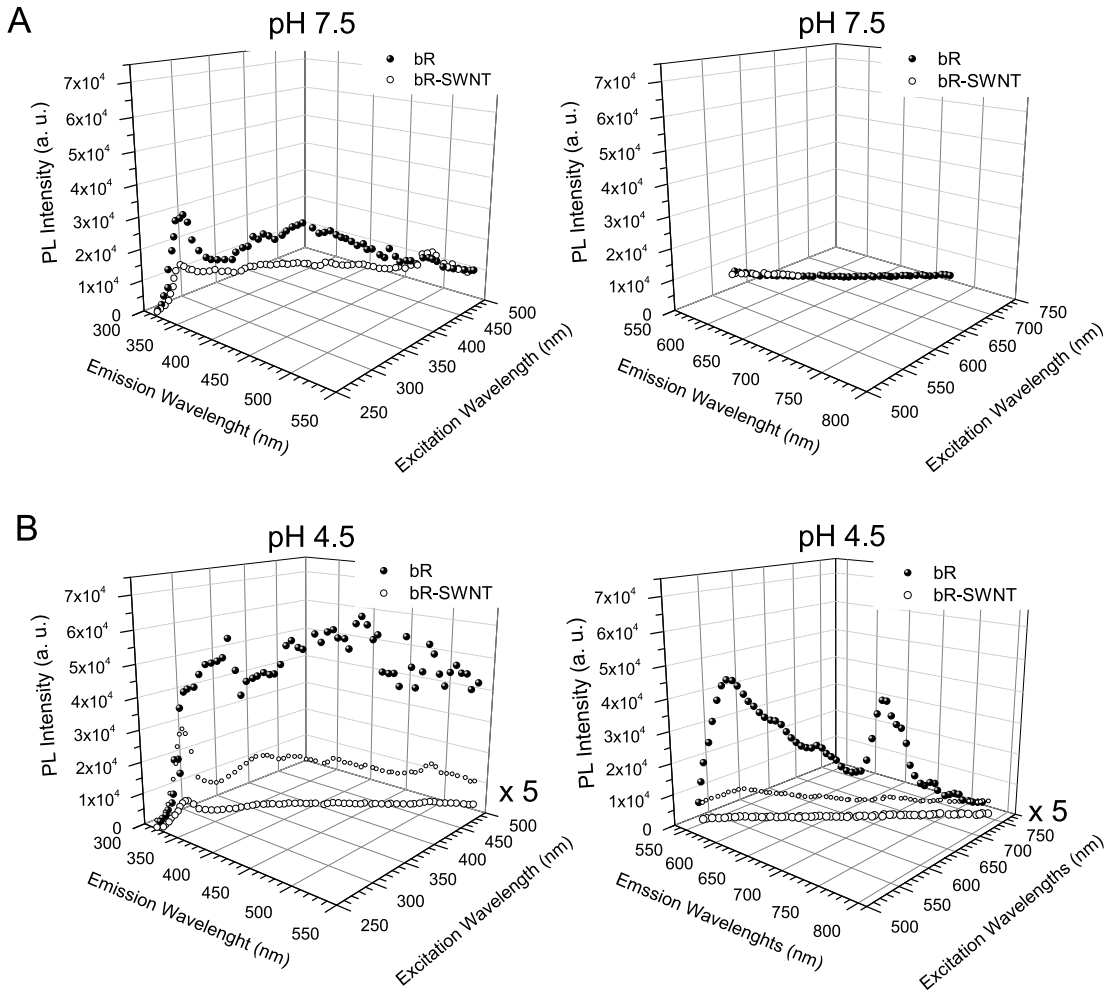

Figure 6. PLE intensity of the maxima of fluorescence for bR alone (black dots) and for SWNT-bR hybrids (open dots) as a function of the emission and excitation wavelengths at pH 7.5 (A) and at pH 4.5 (B). The data for SWNT-bR hybrids at pH 4.5 are also shown with the intensity magnified by a factor 5 (smallest open dots). Data are given for the same amount of protein.

Figure 6B. The ratio between the protein PLE intensity for bR alone and in the presence of SWNTs has been calculated for excitation wavelengths ranging from 298 to 502 nm and 540 to 696 nm, corresponding to the region of spectral overlap. This ratio is equal to 0.062 ± 0.013 (mean value ± standard deviation, $N = 91$). The observed behavior is characteristic of a resonance energy transfer (RET). The efficiency E of a RET process can be derived experimentally from the quenching of the donor fluorescence intensity, according to[34]

$$E = 1 - \frac{F_{DA}}{F_D}$$

where F_D and F_{DA} are the fluorescence of the donor in the absence and presence of an acceptor, respectively. The efficiency E is estimated to range between 92% and 96%.

More fluorescence properties characteristic of the lowest pH values become those of the higher pH values just by increasing the pH of a dispersion containing SWNT–bR hybrids initially at pH 4.5. The reverse situation is valid too.

A nonradiative energy transfer may result from interactions between molecules that can be of Coulombic origin (long-range dipole–dipole and/or short-range multipolar interactions) and/or due to short-range intermolecular orbital overlap. The distances that exist between the chromophoric center of a bR coupled to a SWNT in a SWNT–bR hybrid are less than 8–10 nm whatever the pH value of the buffer solution according to the measurements performed on the AFM images. These distances thus allow considering a resonance energy transfer in the hybrids. It is likely that the SWNT–bR hybrids will have electrostatic charges brought by the coupled proteins. In fact, it is well known that, once coated by electrolytes, pristine carbon nanotubes tend to be charged.[35] Actually electrostatic repulsive forces between coated SWNTs maintain them dispersed in buffer solution and explain the stability of the dispersion. No significant difference in the morphology of the SWNT–bR hybrids has been highlighted as a function of the pH of the buffer solution, but the experiments in which the chromophoric center of

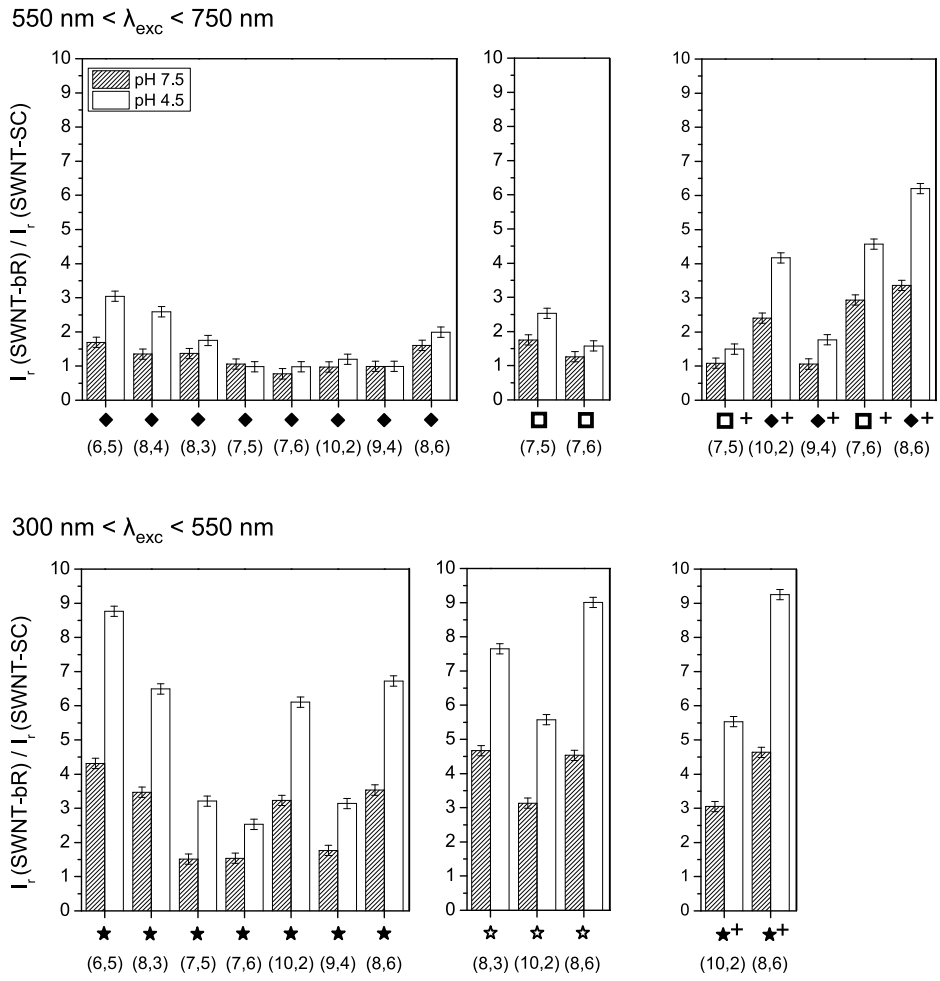

Figure 7. Bar graphs showing the ratio *R* between I_r for a SWNT−bR dispersion at a given pH value and I_r for well-dispersed SWNTs by sodium cholate (SC) at pH 7.5. *R* is equal to 1 for a SWNT−SC dispersion. Specific measurement points are indicated under each bar. Crosses mark points where energy transfer occurs at pH 4.5. Solid diamonds represent the E_{11} emission of SWNTs through the E_{22} excitations of several SWNT species, and open squares denote $E_{12,21}$ transverse photoexcitations. Stars and open stars represent the E_{11} emission of SWNTs through the E_{33} and E_{44} excitations, respectively.

the proteins was removed permit us to demonstrate that the resonance energy transfer observed at pH values lower than 5 is indeed correlated to the presence of the retinylidene molecule in the core of the proteins.

The effect of the pH value is explained in the following way. The emission of bR above 600 nm is attributed to the first allowed excited state of the retinylidene chromophore, irrespective of pH.[25] However, it has been shown that the retinylidene chromophore has three absorption bands: a main band whose maximum occurs at ~565 nm at neutral pH (~605 nm at acidic pH), a weak band at ~400 nm (420 nm at acidic pH), and a very weak band occurring at 300 nm, which extends to 360 nm.[25] Only the fluorescence emission of the main absorption band and the very weak one overlap with the absorption of several SWNT species, which is consistent with our results. The fluorescence maximum at pH 4.5 is blue-shifted by ~10 nm compared to the one at pH 7.5 for excitation wavelengths ranging from 530 to 640 nm (using the data of Figure 6). This is in favor of the presence of one acidic form of bR, called bR^{acid}_{blue}.[25,36] It has been shown that, by decreasing the pH to acidic values (pH < 5), acidic forms of bR begin to appear.[37,38] In particular, the acidic form bR^{acid}_{blue}, absorbing around 605−610 nm with p*K* = 2.9, can be formed at low ionic strength by lowering the pH of the buffer solution; its concentration reaches its maximum at pH 2.[37] The shift of the absorption band to 605−610 nm is associated with the protonation of aspartic acid Asp85 located in the close vicinity of the retinal.[39] Importantly, bR^{acid}_{blue} has a significantly higher fluorescence quantum yield than other forms.[25] So, even present in a very small quantity, the fluorescence emission of bR^{acid}_{blue} is detectable.[36] In addition, the magnitude of the Stokes shift is pH-dependent, larger at neutral pH compared to acidic pH due to a charge displacement induced after excitation which does not exist at acidic pH (bR^{acid}_{blue} does not pump protons).[25,37,38] This has a direct consequence: the acidic form bR^{acid}_{blue} dominates the fluorescence emission above 700 nm even if it is present in a mixture of several bR forms with a very low concentration.[36]

Therefore, for excitation wavelengths ranging from 660 to 680 nm, the fluorescence emission is expected to be considerably enhanced at pH 4.5 compared to pH 7.5 due to the presence of the acidic form bR^{acid}_{blue} species even if it is present in a mixture with other forms with a very low concentration. Thus, our data point to the presence of both the acidic form bR^{acid}_{blue}, which exhibits a high fluorescence quantum yield, and the neutral form bR_{568} (present at pH 7), with low fluorescence quantum yield, at pH 4.5. The fluorescence properties of the SWNT–bR hybrids and their specific pH-dependence can be associated with the specific fluorescence properties of the bR and the possibility of a protonation of the aspartic acid Asp85 located close to the retinal at low pH.

CONCLUSION

In summary, dispersions containing noncovalently functionalized SWNTs by bacteriorhodopsins were obtained using a sodium cholate suspension–dialysis method that preserves the intrinsic properties of both molecules. The dispersions are stable in a wide pH range: from 4.2 to 9. The study reveals not only that energy transfer occurs from bacteriorhodopsins to SWNTs when proteins are photoexcited but also that the mechanism of energy transfer is pH-dependent. So, for pH ranging from 4.2 to 5, luminescence from SWNTs when excited across the protein's optical absorption peaks is observed with characteristics specific to a mechanism of resonance energy transfer. Additional fluorescence features emitted by SWNTs appear at excitation wavelengths between 660 and 680 nm and around 330 nm. The RET efficiency is equal to 0.94. For a pH value higher than 5, radiative energy transfer takes place in which photons emitted by the tryptophan residues of the protein are absorbed by SWNTs. This leads to a strong increase of the intensity of the E_{11} emissions of SWNTs through their E_{33} and E_{44} excitations. Our study not only shows the existence of an energy transfer from bR to SWNTs but also highlights the role of the bacteriorhodopsin in the energy transfer processes between both molecules as a function of the pH. It opens an easy way for enhancing and adjusting the luminescence intensity of the E_{11} emissions of SWNTs through their E_{33} and E_{44} excitations and for adding new excitation wavelengths for SWNTs. The properties of SWNT–bR hybrids are promising for light-harvesting and optoelectronic applications.

METHODS

Commercially available HipCO SWNTs have been purchased from Unidym (batch P0261) (Sunnyvale, CA, USA) and used as received. Suspensions of purple membranes (PM) containing wild-type bR were a courtesy gift from Dieter Oesterhelt's group at the Max-Planck Institute of Biochemistry, Martinsried, Germany. HEPES (4-(2-hydroxyethyl)piperazine-1-ethanesulfonic acid), sodium cholate, TRIS, sodium acetate, acetic acid, potassium phosphate monobasic, sodium hydroxide, hydrochloric acid, and sodium cholate have been purchased from Sigma-Aldrich. Depending on the desired pH, we prepared acetate buffers (pH from 4 to 6), phosphate buffers (pH 6 to 6.8), HEPES buffers (pH from 7 to 8), and TRIS-HCl buffers (pH from 8 to 9).

For sample preparation, we followed a sodium cholate suspension–dialysis method as described by N. R. Palwai *et al.*[20] First a suspension of SWNTs was prepared by adding 0.5 mg of pristine nanotubes to 1 mL of a 2 wt % aqueous solution of sodium cholate. The SWNTs were then dispersed by cup horn sonication for 15 min and bath sonication for 3 h. The preparation was then centrifuged at 7200*g* for 2 h, and the supernatant recovered. Then 3 μL of a suspension of PM at 49 OD was added to 1 mL of the SWNT dispersion, and dialysis using a 10 kDa dialysis membrane (Spectrum Laboratories) was carried out at the desired pH value for 6 h to remove sodium cholate. The resulting solution was transferred to a 100 kDa dialysis membrane (Spectrum Laboratories) and dialyzed against 500 mL of buffer at the desired pH value for 1 h to remove excess proteins. Finally the suspension was centrifuged at 7200*g* for 30 min. A control experiment was also performed in which no protein was added. The removal of sodium cholate molecules using a 10 kDa dialysis membrane for the same time duration and pH conditions leads to a completely destabilized dispersion.

The dispersions were characterized by Fourier-transform Raman spectroscopy (FT-Raman) using an RFS 100 Bruker FT spectrometer and a Nd:YAG laser working at 1064 nm.

Atomic force microscopy (AFM) images were recorded in buffer solution with a Nanowizard II AFM (JPK Instruments AG, Berlin, Germany) using silicon nitride tips (OTR4, Bruker AFM probes). Images were taken in an intermittent contact mode with very low driven amplitudes and scan rates below 0.5 Hz. Heights on AFM images were measured using WSXM software routines.[40] Sample preparation for AFM observations consists of the deposition of 20 μL of supernatant containing SWNT–bR hybrids at a given pH onto a freshly cleaved mica surface for 15 min, rinsing of the surface with ultrapure water, and drying under N_2 flux. The sample surface was then completely immerged in buffer solutions at the same pH before imaging. Images in Figure 2 were recorded in a buffer solution at pH 4.5 from dispersion at the same pH. Similar results were found for pH 7.5.

UV–vis–NIR absorption spectra of the dispersions were recorded on a CARY 5G UV–vis–NIR spectrometer. We follow the procedure described by R. Haggenmueller *et al.*[41] for determining the concentration of SWNTs. The concentration of bR was calculated by subtracting contributions of SWNTs to the absorbance at 568 nm and using an extinction coefficient of 63 000 M^{-1} cm^{-1}. The ratio between the mass concentrations of SWNTs and proteins in the dispersions was around 2.1 whatever the pH.

Photoluminescence excitation/emission maps and fluorescence spectra were performed with a Jobin-Yvon Horiba Fluorolog spectrometer using a UV–visible xenon lamp as excitation source. The detectors were a CCD camera for the UV–visible range and an InGaAs for the infrared range (427C-AU Horiba). For the measurements of the fluorescence emission of the tryptophan residues under illumination, an external laser diode was used with a wavelength of 561 nm. The excitation wavelength chosen was 288 nm in the presence of a high pass filter (wavelengths $\geq$320 nm). Fluorescence spectra of bacteriorhodopsin were in agreement with previous studies.[42,43]

Conflict of Interest: The authors declare no competing financial interest.

Supporting Information Available: Additional figures. This material is available free of charge *via* the Internet at http://pubs.acs.org.

Acknowledgment. Suspensions of PM-containing wild-type bR were a gift from D. Oesterhelt's group at Max-Planck Institute of Biochemistry, Martinsried, Germany.

REFERENCES AND NOTES

1. Boghossian, A. A.; Zhang, J.; Barone, P. W.; Reuel, N. F.; Kim, J.-H.; Heller, D. A.; Ahn, J.-H.; Hilmer, A. J.; Rwei, A.; Arkalgud, J. R.; *et al*. Near-Infrared Fluorescent Sensors Based on Single-Walled Carbon Nanotubes for Life Sciences Applications. *Chem. Sus. Chem.* **2011**, *4*, 848–863.
2. Lefebvre, J.; Maruyama, S.; Finnie, P. Photoluminescence: Science and Applications. *Top. Appl. Phys.* **2008**, *111*, 287–319.
3. Zhang, L.; Tabakman, S.; Welsher, K.; Dai, H. Carbon Nanotubes in Biology and Medecine: *in Vitro* and *in Vivo* Detection, Imaging and Drug Delivery. *Nano Res.* **2009**, *2*, 85–120.
4. Kim, J.-H.; Heller, D. A.; Jin, H.; Barone, P. W.; Song, C.; Zhang, J.; Trudel, L. J.; Wogan, J. N.; Tannenbaum, S. R.; Strano, M. S. The Rational Design of Nitric Oxide Selectivity in Single-Walled Carbon Nanotube Near-Infrared Fluorescence Sensors for Biological Detection. *Nat. Chem.* **2009**, *1*, 473–481.
5. Zhou, F.; Xing, D.; Wu, B.; Wu, S.; Ou, Z.; Chen, W. R. New Insights of Transmembranal Mechanism and Subcellular Localization of Noncovalently Modified Single-Walled Carbon Nanotubes. *Nano Lett.* **2010**, *10*, 1677–1681.
6. Robinson, J. T.; Hong, G.; Liang, Y.; Zhang, B.; Yaghi, O. K.; Dai, H. *In Vivo* Fluorescence Imaging in the Second Near-Infrared Window with Long Circulating Carbon Nanotubes Capable of Ultrahigh Tumor Uptake. *J. Am. Chem. Soc.* **2012**, *134*, 10664–10669.
7. Ehli, C.; Oelsner, C.; Guldi, D. M.; Mateo-Alonso, A.; Prato, M.; Schmidt, C.; Backes, C.; Hauke, F.; *et al*. Manipulating Single-Wall Carbon Nanotubes by Chemical Doping and Charge Transfer with Perylene Dyes. *Nat. Chem.* **2009**, *1*, 243–249.
8. Ehli, C.; Aminur Rahman, G. M.; Jux, N.; Balbinot, D.; Guldi, D. M.; Paolucci, F.; Marcaccio, M.; Paolucci, D.; Melle-Franco, M.; Zerbetto, F.; *et al*. Interactions in Single Wall Carbon Nanotubes/Pyrene/Porphirin Nanohybrids. *J. Am. Chem. Soc.* **2006**, *128*, 11222–11231.
9. Campidelli, S.; Ballesteros, B.; Filoramo, A.; Diaz Diaz, D.; de la Torre, G.; Torres, T.; Aminur Rahman, G. M.; Ehli, C.; Kiessling, D.; Werner, F.; *et al*. Facile Decoration of Functionalized Single-Wall Carbon Nanotubes with Phtalocyanines *via* "Click Chemistry". *J. Am. Chem. Soc.* **2008**, *130*, 11503–11509.
10. Roquelet, C.; Garrot, D.; Lauret, J. S.; Voisin, C.; Alain-Rizzo, V.; Roussignol, Ph.; Delaire, J. A.; Deleporte, E. Quantum Efficiency of Energy Transfer in Noncovalent Carbon Nanotube/Porphyrin Compounds. *App. Phys. Lett.* **2010**, *97*, 141918.
11. Hu, L.; Zhao, Y.-L.; Ryu, K.; Zhou, C.; Fraser Stoddart, J.; Grüner, G. Light-Induced Charge Transfer in Pyrene/CdSe-SWNT Hybrids. *Adv. Mater.* **2008**, *20*, 939–946.
12. Umeyama, T.; Kadota, N.; Tezuka, N.; Matano, Y.; Imahori, H. Photoinduced Energy Transfer in Composites of Poly[(*p*-phenylene-1,2-vinylene)-*co*-(*p*-phenylene-1,1-vinylidene)] and Single-Walled Carbon Nanotubes. *Chem. Phys. Lett.* **2007**, *444*, 263–267.
13. Chen, F.; Zhang, W.; Jia, M.; Wei, L.; Fan, X.-F.; Kuo, J.-L.; Chen, Y.; Chan-Park, M. B.; Xia, A.; *et al*. Energy Transfer from Photo-Excited Fluorene Polymers to Single-Walled Carbon Nanotubes. *J. Phys. Chem. C* **2009**, *113*, 14946–14952.
14. Dorogi, M.; Balint, Z.; Miko, C.; Vileno, B.; Milas, M.; Hernadi, K.; Forro, L.; Varo, G.; Nagy, L. Stabilization Effect of Single-Walled Carbon Nanotubes on the Functioning of Photosynthetic Reaction Centers. *J. Phys. Chem. B* **2006**, *110*, 21473–21479.
15. Kaniber, S. M.; Brandstetter, M.; Simmel, F. C.; Carmeli, I.; Holleitner, A. W. On-Chip Functionalization of Carbon Nanotubes with Photosystem I. *J. Am. Chem. Soc.* **2010**, *132*, 2872–2873.
16. Ham, M.-H.; Choi, J. H.; Boghossian, A. A.; Jeng, E. S.; Graff, R. A.; Heller, D. A.; Chang, A. C.; Mattis, A.; Bayburt, T. H.; Grinkova, Y. V.; *et al*. Photoelectrochemical Complexes for Solar Energy Conversion that Chemically and Autonomously Regenerate. *Nat. Chem.* **2010**, *2*, 929–936.
17. Giardi, M. T.; Pace, E. Photosynthetic Proteins for Technological Applications. *Trends Biotechnol.* **2005**, *23*, 257–263.
18. Hampp, N. A. Bacteriorhodopsin: Mutating a Biomaterial into an Optoelectronic Material. *Appl. Microbiol. Biotechnol.* **2000**, *53*, 633–639.
19. Bertoncini, P.; Chauvet, O. Conformational Structural Changes of Bacteriorhodopsin Adsorbed onto Single-Walled Carbon Nanotubes. *J. Phys. Chem. B* **2010**, *114*, 4345–4350.
20. Palwai, N. R.; Martyn, D. E.; Neves, L. F. F.; Tan, Y.; Resasco, D. E.; Harrison, R. G. Retention of Biological Activity and Near-Infrared Absorbance upon Absorption of Horseradish Peroxidase on Single-Walled Carbon Nanotubes. *Nanotechnology* **2007**, *18*, 235601–235605.
21. O'Connell, M. J.; Bachilo, S. M.; Huffman, C. B.; Moore, V. C.; Strano, M. S.; Haroz, E. H.; Rialon, K. L.; Boul, P. J.; Noon, W. H.; Kittrell, C.; *et al*. Band Gap Fluorescence from Individual Single-Walled Carbon Nanotubes. *Science* **2002**, *297*, 593–596.
22. Bachilo, S. M.; Strano, M. S.; Kittrell, C.; Hauge, R. H.; Smalley, R. E.; Weisman, R. B. Structure-Assigned Optical Spectra of Single-Walled Carbon Nanotubes. *Science* **2002**, *298*, 2361–2366.
23. Oesterhelt, D.; Hess, B. Reversible Photolysis of the Purple Complex in the Purple Membrane of *Halobacterium Halobium*. *Eur. J. Biochem.* **1973**, *37*, 316–326.
24. Gergely, C.; Zimanyi, L.; Varo, G. Bacteriorhodopsin Intermediate Spectra Determined over a Wide pH Range. *J. Phys. Chem. B* **1997**, *101*, 9390–9395.
25. Kouyama, T.; Kinosita, K., Jr.; Ikegami, A. Excited-State Dynamics of Bacteriorhodopsin. *Biophys. J.* **1985**, *47*, 43–54.
26. Weisman, R. B.; Bachilo, S. M. Dependence of Optical Transition Energies on Structure for Single-Walled Carbon Nanotubes in Aqueous Suspension: An Empirical Kataura Plot. *Nano Lett.* **2003**, *3*, 1235–1238.
27. Haroz, E. H.; Bachilo, S. M.; Weisman, R. B.; Doorn, S. K. Curvature Effects on the E_{33} and E_{44} Exciton Transitions in Semiconducting Single-Walled Carbon Nanotubes. *Phys. Rev. B* **2008**, *77*, 125405–125413.
28. Lebedkin, S.; Hennrich, F.; Kiowski, O.; Kappes, M. M. Photophysics of Carbon Nanotubes in Organic Polymer-Toluene Dispersions: Emission and Excitation Satellites and Relaxation Pathways. *Phys. Rev. B* **2008**, *77*, 165429–165436.
29. Miyauchi, Y.; Oba, M.; Maruyama, S. Cross-Polarized Optical Absorption of Single-Walled Nanotubes by Polarized Photoluminescence Excitation Spectroscopy. *Phys. Rev. B* **2006**, *74*, 205440–205445.
30. Green, A. A.; Duch, M. C.; Hersam, M. C. Isolation of Single-Walled Carbon Nanotube Enantiomers by Density Differentiation. *Nano Res.* **2009**, *2*, 69–77.
31. Lefebvre, J.; Finnie, P. Polarized Photoluminescence Excitation Spectroscopy of Single-Walled Carbon Nanotubes. *Phys. Rev. Lett.* **2007**, *98*, 167406–167409.
32. Oesterhelt, D.; Schuhmann, L.; Gruber, H. Light-Dependent Reaction of Bacteriorhodopsin with Hydroxylamine in Cell Suspensions of *Halobacterium Halobium*: Demonstration of an Apo-Membrane. *FEBS Lett.* **1974**, *44*, 257–261.
33. Oesterhelt, D.; Schuhmann, L. Reconstitution of Bacteriorhodopsin. *FEBS Lett.* **1974**, 262–265.
34. Valeur, B. *Molecular Fluorescence: Principles and Applications*, 2nd ed.; Wiley-VCH, 2012.
35. Sun, Z.; Nicolosi, V.; Rickard, D.; Bergin, S. D.; Aherne, D.; Coleman, J. N. Quantitative Evaluation of Surfactant-Stabilized Single-Walled Carbon Nanotubes: Dispersion Quality and Its Correlation with Zeta Potential. *J. Phys. Chem. C* **2008**, *112*, 10692–10699.
36. Schenkl, S.; Portuondo, E.; Zgrablic, G.; Chergui, M.; Suske, W.; Dolder, M.; Landau, E. M.; Haacke, S. Compositional Heterogeneity Reflects Partial Dehydration in Three-Dimensional Crystals of Bacteriorhodopsin. *J. Mol. Biol.* **2003**, *329*, 711–719.
37. Mowery, P. C.; Lozier, R. H.; Chae, Q.; Tseng, Y.-W.; Taylor, M.; Stoeckenius, W. Effect of Acid pH on the Absorption Spectra and Photoreactions of Bacteriorhodopsin. *Biochemistry* **1979**, *18*, 4100–4107.

38. Varo, G.; Lanyi, J. K. Photoreactions of Bacteriorhodopsin at Acid pH. *Biophys. J.* **1989**, *56*, 1143–1141.
39. Metz, G.; Siebert, F.; Englehard, M. Asp85 id the Only Internal Aspartic Acid that Gets Protonated in the M Intermediate and the Purple-to-Blue Transition of Bacteriorhodopsin. A Solid-State ^{13}C CP-MAS NMR Invstigation. *FEBS Lett.* **1992**, *2*, 237–241.
40. Horca, I.; Fernandez, R.; Gomez-Rodriguez, J. M.; Colchero, J.; Gomez-Herrero, J.; Baro, A. M. WSXM: A Software for Scanning Probe Microscopy and a Tool for Nanotechnology. *Rev. Sci. Instrum.* **2007**, *78*, 13705–13712.
41. Haggenmueller, R.; Rahatekar, S. S.; Fagan, J. A.; Chun, J.; Becker, M. L.; Naik, R. R.; Krauss, T.; Carlson, L.; Kadla, J. F.; Trulove, P. C.; *et al*. Comparison of the Quality of Aqueous Dispersions of Single Wall Carbon Nanotubes Using Surfactants and Biomolecules. *Langmuir* **2008**, *24*, 5070–5078.
42. Schenkl, S.; Zgrablic, G.; Portuondo-Campa, E.; Haacke, S.; Chergui, M. On the Excitation Wavelength Dependence of the Fluorescence of Bacteriorhodopsin. *Chem. Phys. Lett.* **2007**, *441*, 322–326.
43. Haacke, S.; Vinzani, S.; Schenkl, S.; Chergui, M. Spectral and Kinetic Fluorescence Properties of Native and Noninsomerizing Retinal in Bacteriorhodopsin. *Chem. Phys. Chem.* **2001**, *2*, 310–315.